Supporting Information for

Electrochemical Oxidation of Styrene to Benzaldehyde by Discrimination of Spin-Paired π Electrons

Xiaoxue Luo,[a] Xiaoxia Tang,[a] Jingtian Ni,[a] Baijing Wu,[a] Cunpu Li,[*,a] Minhua Shao,[b] and Zidong Wei[*,a]

[a] The State Key Laboratory of Power Transmission Equipment & System Security and New Technology, Chongqing Key Laboratory of Chemical Process for Clean Energy and Resource Utilization, College of Chemistry and Chemical Engineering, Chongqing University, Chongqing, 400044, China.

[b] Department of Chemical and Biological Engineering, The Hong Kong University of Science and Technology, Clear Water Bay, Kowloon, Hong Kong.

E-mail: lcp@cqu.edu.cn; zdwei@cqu.edu.cn

1. Method and Synthesis

1.1 Catalytic Electrode Preparation

The bright Ti electrode substrate was obtained by using the 3 mol L^{-1} H_2SO_4 at 80ºC for 1 h to remove the oxides and impurities on the surface. Then the electrode was sequentially washed in acetone, ethanol, subsequently, and stored in isopropanol solution until use.

The anode electrode was firstly prepared with RuO_2 and TiO_2 coating on Ti mesh by thermochemical oxidation deposition method using a mixture of $RuCl_3$ and $C_{16}H_{36}O_4Ti$ dissolved in isopropanol. Specifically, the total metal loading was controlled to 32.97 μmol cm^{-2}, and the molar ratios of Ru and Ti metal ions were adjusted to 3:7, 2:8, 1:9, and 0.5:9.5, respectively.

Firstly, the pretreated Ti meshes were brushed with the mixtures of $RuCl_3$ and $C_{16}H_{36}O_4Ti$ solutions. The Ti meshes were then put into a furnace for drying at 400 ºC for 10 minutes, to make the solvent volatilize. This step was repeated until all the mixture is coated on the electrode surface and the desired metal loading achieved. After that, the as-prepared electrodes were annealed at 500ºC for 1 h under ambient air. Then the obtained electrodes were cleaned with ethanol and DI water. The obtained electrodes were denoted as $(Ru_xTi_{1-x})O_2$/Ti (x=0.3, 0.2, 0.1, 0.05), where x is the corresponding molar proportion of Ru.

The MnO_2 catalytic layer were coated onto the electrodes by electrodeposition oxidation method. After washing the prepared $(Ru_xTi_{1-x})O_2$/Ti (x=0.3, 0.2, 0.1, 0.05) electrodes, the electrodes were put into a manganese-containing electrolyte for electro-oxidative deposition experiments. The electrolyte composition was 1 M $MnSO_4$ H_2O containing 0.1 M H_2SO_4, and the current density was controlled at 6 mA cm^{-2}. The electrodeposition deposition was performed at 60ºC for 2 h. The finally obtained electrodes were donated as MnO_2/$(Ru_xTi_{1-x})O_2$/Ti (x=0.3, 0.2, 0.1, 0.05), respectively.

For comparison, an electrode that MnO_2 was deposited directly on Ti mesh (MnO_2/Ti) was prepared. Also, spin-symmetric TiO_2 and MoO_3 materials, as well as spin-asymmetric MoO_2, were introduced on-

to $(Ru_{0.3}Ti_{0.7})O_2$/Ti. The TiO_2 and MoO_3 were introduced through thermal decomposition method by using the same $C_{16}H_{36}O_4Ti$ solution (metal ions remained at 32.97 μmol cm^{-2}). The ammonium molybdate was used as the MoO_3 precursor. the MoO_2 was prepared through ammonium molybdate electrodeposition reduction method. The electrolyte was composed of 1 mol/L NH_4^+ and 0.05 mol/L ammonium molybdate, and the pH controlled to be 7.0. The voltage maintained at -1.5 V (*vs.* SCE) for 2 h at 30°C. The obtained electrodes were named as TiO_2/$(Ru_{0.3}Ti_{0.7})O_2$/Ti, MoO_3/$(Ru_{0.3}Ti_{0.7})O_2$/Ti and MoO_2/$(Ru_{0.3}Ti_{0.7})O_2$/Ti, respectively.

The surface morphology, crystal structure, and elemental information of the electrodes were analyzed by X-ray diffraction (Model XRD-6000, Shimadzu), field-emission scanning electron microscopy (FE-SEM) (Model JSM-7800, JEOL, Tokyo, Japan), transmission electron microscopy (TEM), scanning TEM (STEM) and energy-dispersive X-ray spectroscopy (EDX), electron paramagnetic resonance (EPR) (Bruker EMX PLUS) and X-ray photoelectron spectroscopy (XPS) (Thermo-Fisher). Ru and Ti elemental analysis of the prepared electrodes were performed with the Electron Probe MicroAnalysis (EPMA) method. The *in-situ* XPS measurement was performed on Thermo-Fisher (ESCALAB 250Xi).

1.2 Electrochemical Measurements

Electrochemical measurements were conducted through a CHI1140C electrochemical workstation in a H-type electrolytic cell and using the three-electrode electrochemical system. The MnO_2/$(Ru_xTi_{1-x})O_2$/Ti (where x=0.3, 0.2, 0.1, 0.05) electrodes, with a geometric area of 1.5 cm × 1 cm were individually used as working electrodes. In all comparative experiments, the working electrodes area kept the same as the MnO_2/$(Ru_xTi_{1-x})O_2$/Ti (where x=0.3, 0.2, 0.1, 0.05). Ag/AgCl (saturated KCl) electrode was used as the reference, and a Pt sheet (1 cm × 1 cm) was used as the counter electrode, respectively. Unless otherwise stated, all the potentials in this research were relative to as RHE ($E_{RHE} = E_{Ag/AgCl} + 0.059pH$). Linear sweep voltammetry (LSV) curves were recorded at 25°C with a scan rate of 5 mV s^{-1}.

Before testing, the working electrode was activated by cyclic voltammetry to achieve a stable working state. Then, its electrochemical behavior from 1.2 V to 2 V was detected by the LSV method. After that, the reaction was performed by constant potential electrolysis method in the H-cell and anode chambers separated by a Nafion HP membrane (DuPont, 20 μm). Unless otherwise stated, the anode electrolyte composed of 0.3 mmol styrene dissolved in the mixture solution contained 25 mL 0.5 M H_2SO_4 and 5 mL 1,4-dioxane, which was used to increase the solubility of styrene. In each run, the exposed geometric surface area of the working electrode was maintained at 3 cm^2 and using the magnetic stir bar kept the rotating speed at 1000 rpm. The reaction temperature was maintained at 25°C with a water bath.

The electrochemistry *in-situ* attenuated total reflection infrared spectroscopy (ATR-IR) experiment was carried out on the BRUKER VERTEX 70v FT-IR spectrometer equipped with a liquid nitrogen cooled digital MCT detector. To investigate the behavior of electrooxidation reaction on the surface of electrode, the ATR experiment was carried out.[1] The silicon half cylinder serves as the infrared window. At first, the surface of Si half cylinder was polished with Al_2O_3 polishing power until it is completely hydrophobic, and then soaked with piranha solution until the surface is completely hydrophilic. Then the surface was engraved in NH_4F solution until the surface is completely hydrophobic, and finally electroplated in the plating solution containing Au precursor. The prepared Au film should have a uniform, golden appearance, small resistance, and good adhesion.

To prepare the catalyst ink, the catalyst powder was scraped from the $MnO_2/(Ru_{0.3}Ti_{0.7})O_2$/Ti electrode. Then 10 mg of catalyst powder was dispersed in 600 μL ethanol, 380 μL deionized water and 20 μL of a 5 wt % Nafion solution by vigorous sonication. After that the catalyst ink was dropped on the surface of Au film, and dried under the red light to obtain the catalyst layer.

Finally, the infrared window with the catalyst was installed in the special electrochemical *in-situ* spectrum cell, and then the spectrum cell was installed in the infrared device to start the test. During the

test, we commanded the software to collect the spectrum at regular interval of 30 minutes. The infrared spectrum in this paper is expressed in the form of absorbance.

$$\text{Abs.} = -\log\frac{I}{I_0}$$

Where, I and I_0 are the light intensity of sample spectrum and reference spectrum respectively.

1.3 Product Analysis

After the reaction, the anode liquid solution were extracted three times with 5 mL of ethyl acetate and analyzed by gas chromatography (GC,Tianmei GC-7980) with a KBINNOWax capillary column (30 m × 0.32 mm × 0.50 um) and a flame ionization detector (FID). The further detection was conducted by a high-performance liquid chromatographic (HPLC, Shimadzu) equipped with an ultraviolet-visible detector (210 nm) and a Bio-Rad Aminex HPX-87H column (300 mm×7.8 mm). The instrument was operated at 35 °C with an isocratic method at a 0.6 mL^{-1} flow rate. HPLC eluents were 0.008 M H_2SO_4. And farther analyzation was performed through Triple quadrupole GC-MS (SHIMADZU Corporation). The reactant conversion and product selectivity of organic compounds were calculated by the following equations:

$$\text{Conversion}(\%) = \frac{n_S^0 - n_S}{n_S^0} \times 100\% \quad (1)$$

$$\text{Selectivity}(\%) = \frac{n_{BA}}{n_S^0 - n_S} \times 100\% \quad (2)$$

where n_S^0 and n_S are the initial and final amount of styrene, respectively; n_{BA} is the final amount of benzaldehyde. The Faradaic efficiency (FE) for oxidation is calculated by equation 3:

$$\text{FE}(\%) = \frac{n_{BA} \times 4F}{Q} \times 100\% \quad (3)$$

where F is the Faradaic constant and Q is the total consumed charge.

1.4 Density Functional Theory (DFT) Calculation

DFT calculations were performed as implemented in the plane wave set Vienna ab initio Simulation Package (VASP) code.[2] Generalized gradient approximation (GGA) with the exchange-correlation functional in the Perdew-Burke-Ernzerhof (PBE) form was adopted.[3] DFT + U method was used to better describe the on-site coulomb (U) correlation of the localized 3d electrons of Mn with U - J = 4.0 eV, Ti with U - J = 4.0 eV and Mo with U - J = 2.0 eV. An empirical dispersion corrected DFT method (DFT-D3) was carried out to reasonably describe the weak long-distance van der Waals (vdWs) effects.[4, 5] Spin polarization was considered for all calculations. The kinetic-energy cutoff was set as 450 eV. The convergence threshold of 10^{-6} eV was set for self-consistent field (SCF) iteration between two electronic steps. The conjugate gradient method was adopted for geometry optimization with forces on each atom less than 0.02 eV/Å. A p(2×2) unit cell slab model of MnO_2 (131) surface with six MnO_2 atomic layers was used to ensure the large lateral lattice (>1.5 nm). A vacuum layer of 15 Å was inserted along the z-direction to prevent the periodic image interactions. The bottom three atomic layers were fixed although other layers and the adsorbates were fully relaxed during structural optimizations. A k-point mesh of 2× 2×1 was sampled for the Brillouin zone.

The adsorption energy of styrene on MnO_2 surface was calculated by the following equation:

$$\Delta E_{ads} = E_{system} - E_{surface} - E_{styrene} \quad (4)$$

where E_{system}, $E_{surface}$, and $E_{styrene}$ are the total energies of the surface with styrene adsorption, the surface only, and the styrene molecule, respectively.

2. Supporting Figures

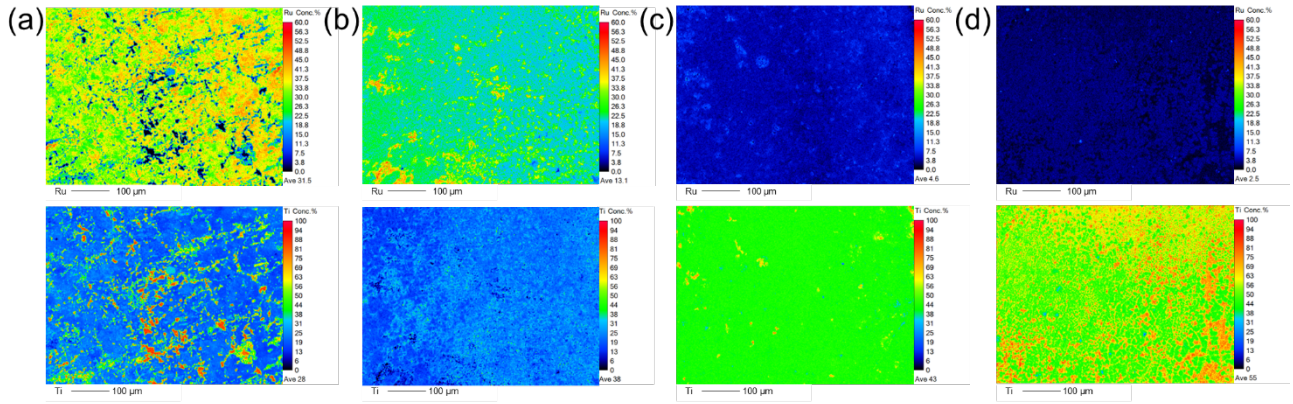

Figure S1. The EPMA images of the actual ratio of Ru and Ti. (a: $(Ru_{0.3}Ti_{0.7})O_2/Ti$, b: $(Ru_{0.2}Ti_{0.8})O_2/Ti$, c: $(Ru_{0.1}Ti_{0.9})O_2/Ti$, d: $(Ru_{0.05}Ti_{0.95})O_2/Ti$).

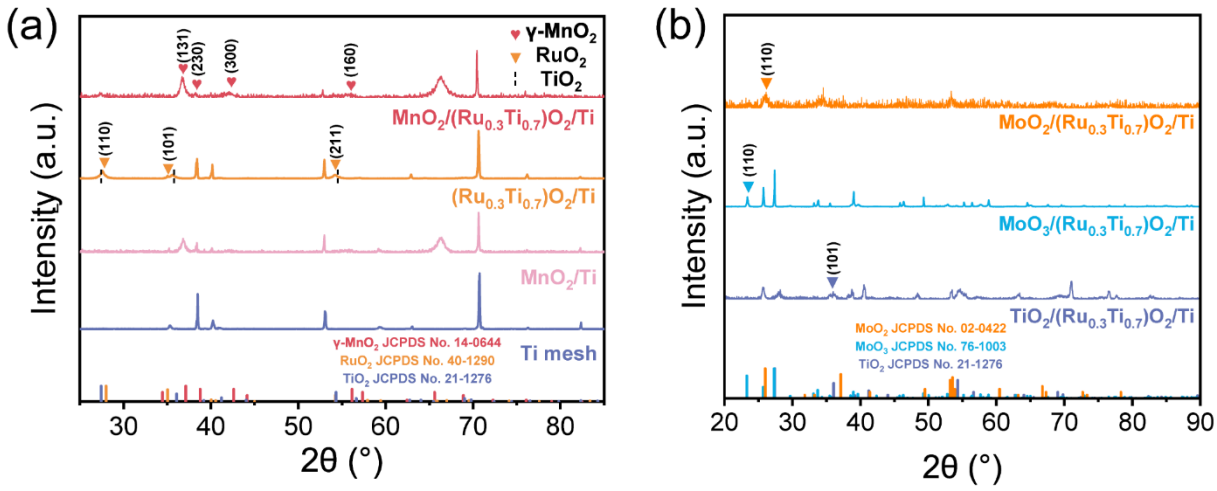

Figure S2. (a-c) XRD patterns of different prepared electrodes.

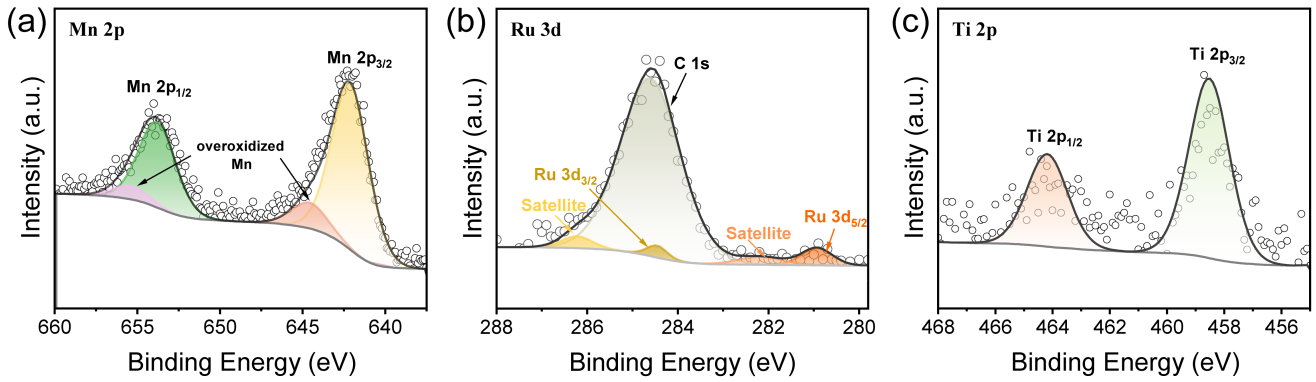

Figure S3. XPS spectra of prepared $MnO_2/(Ru_{0.3}Ti_{0.7})O_2/Ti$ ((a) Mn 2p (b)Ru 3d, (c)Ti 2p).

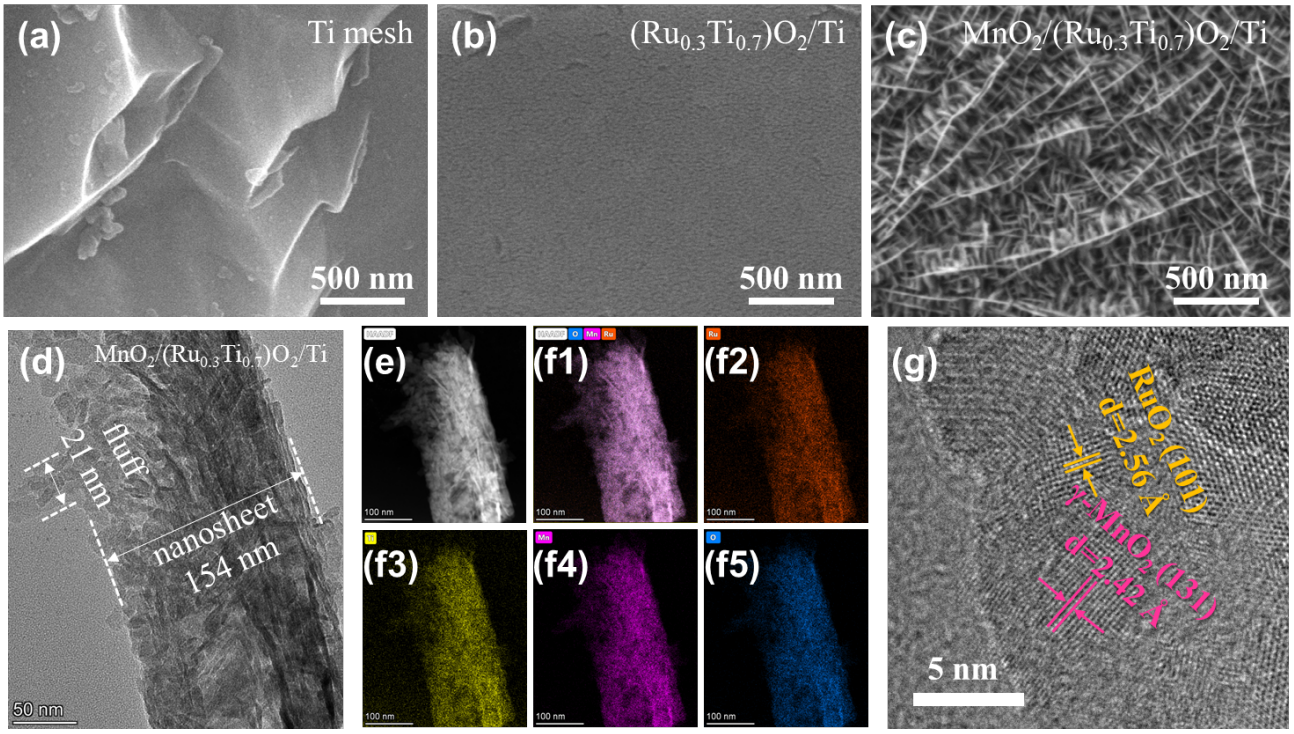

Figure S4. (a-c) SEM images of the prepared catalysts. (a) Ti mesh, (b) $(Ru_{0.3}Ti_{0.7})O_2$/Ti, (C) $MnO_2/(Ru_{0.3}Ti_{0.7})O_2$/Ti. (d-f) TEM images of $MnO_2/(Ru_{0.3}Ti_{0.7})O_2$/Ti. (e) HAADF-STEM image of $MnO_2/(Ru_{0.3}Ti_{0.7})O_2$/Ti; (f1-f5) EDX elemental mapping images; (g) HRTEM image.

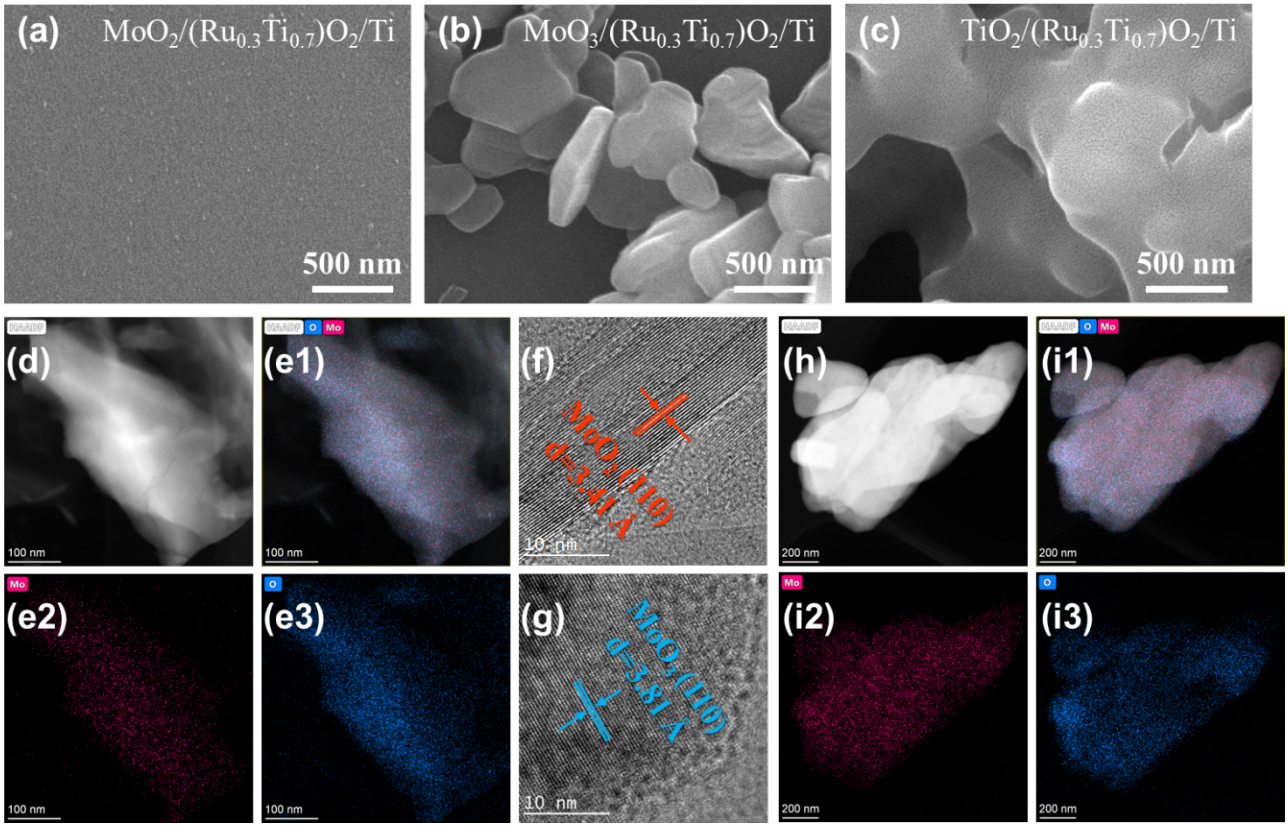

Figure S5. (a-c) SEM images of the prepared catalysts. (a) $TiO_2/(Ru_{0.3}Ti_{0.7})O_2/Ti$, (b) $MoO_3/(Ru_{0.3}Ti_{0.7})O_2/Ti$, (c) $MoO_3/(Ru_{0.3}Ti_{0.7})O_2/Ti$. (d-i) TEM images of $MoO_3/(Ru_{0.3}Ti_{0.7})O_2/Ti$ and $MoO_2/(Ru_{0.3}Ti_{0.7})O_2/Ti$. (d) and (h) HAADF-STEM image; (e1-e3) and (i1-i3) EDX elemental mapping images; (f-g) HRTEM image.

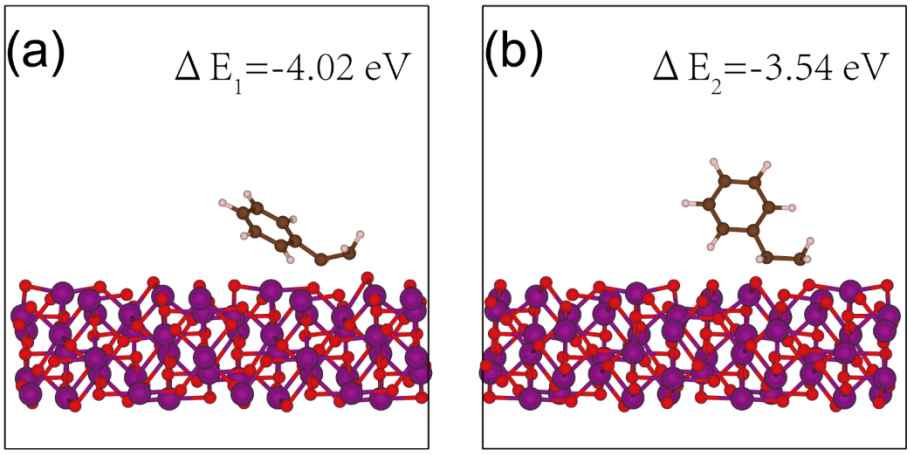

Figure S6. (a-b) Two different adsorption postures of styrene after DFT calculation on MnO_2(131).

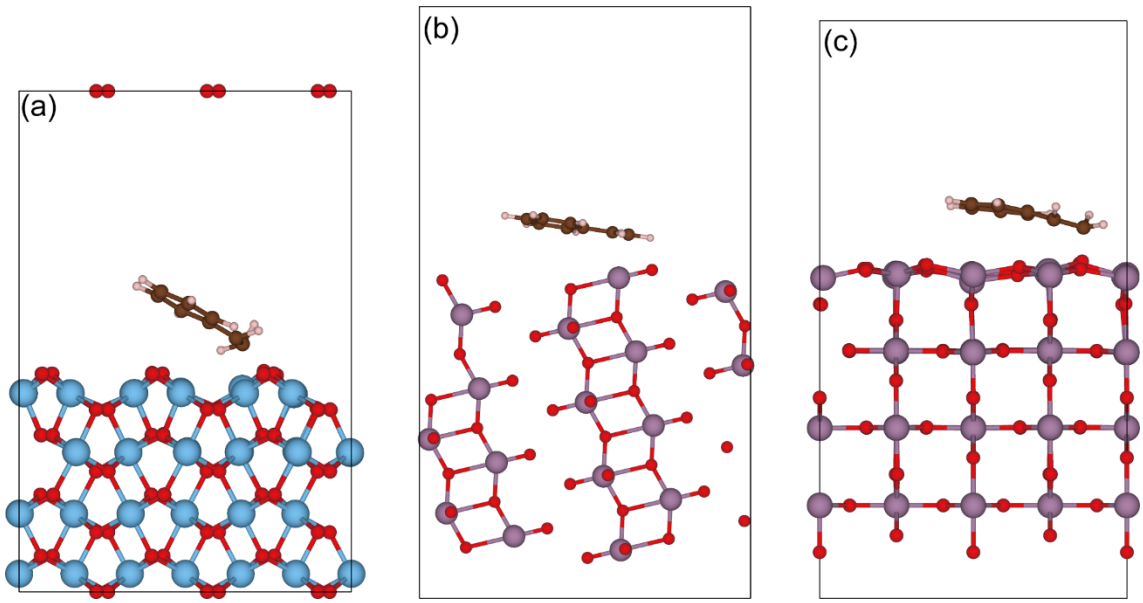

Figure S7. The adsorption of styrene after DFT calculation on TiO_2(101), MoO_3(110) and MoO_2(110).

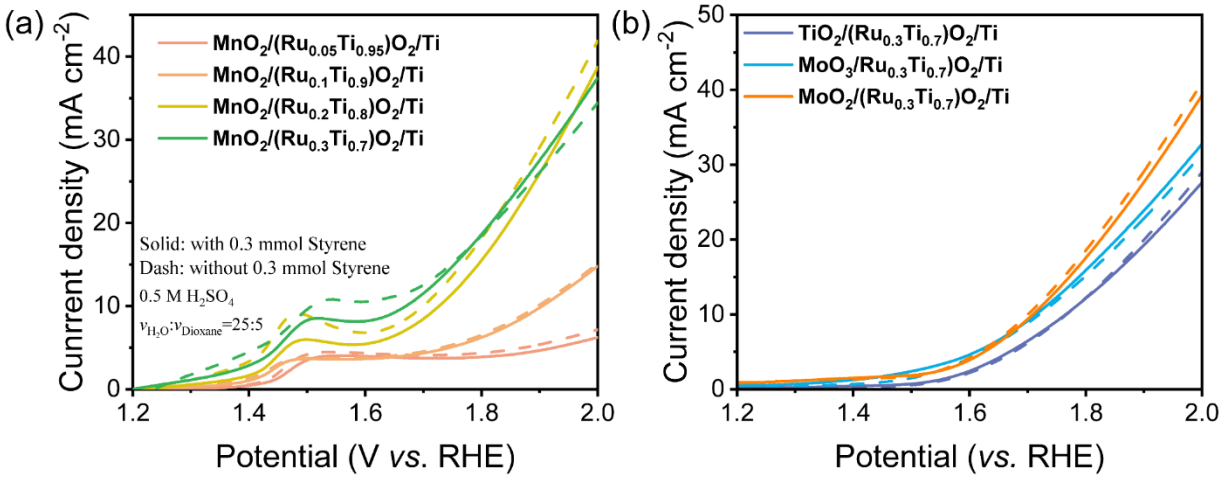

Figure S8. LSV curves of the different materials electrodes grown on Ti mesh at a scan rate of 5 mV s^{-1} in 0.5 M H_2SO_4 and 1,4-dioxane co-solvents (v_1: v_2 =25:5) with (solid lines) and with-out (dash lines) the presence of 0.3 mmol Styrene.

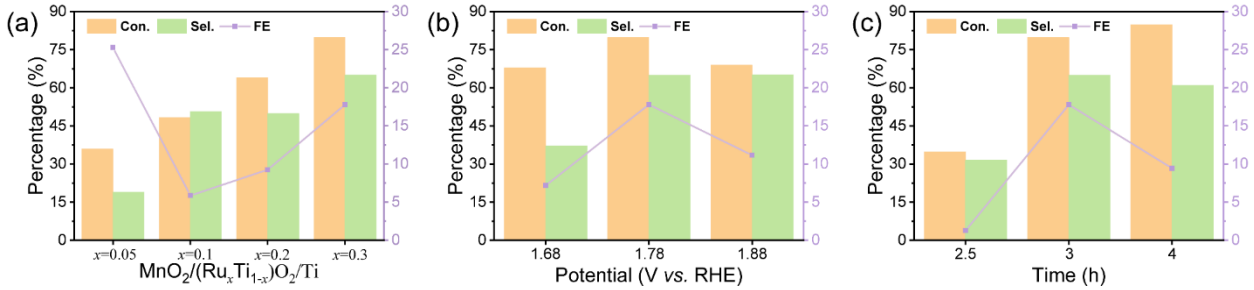

Figure S9. The optimizations of reaction conditions (Time and Potential).

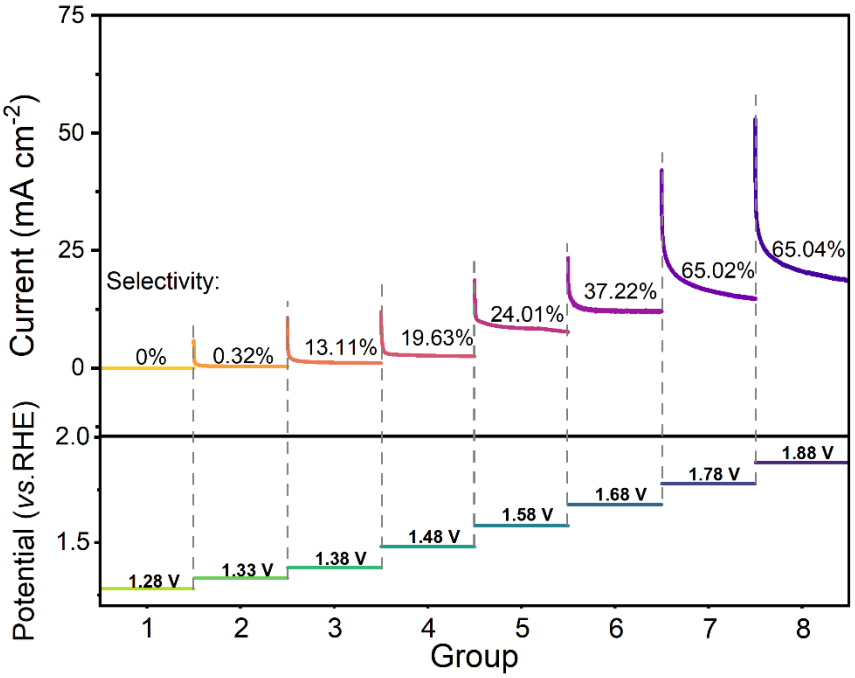

Figure S10. The I-t curves and selectivity of benzaldehyde at different potentials (*vs.* RHE) using $MnO_2/(Ru_{0.3}Ti_{0.7})O_2/Ti$ electrode.

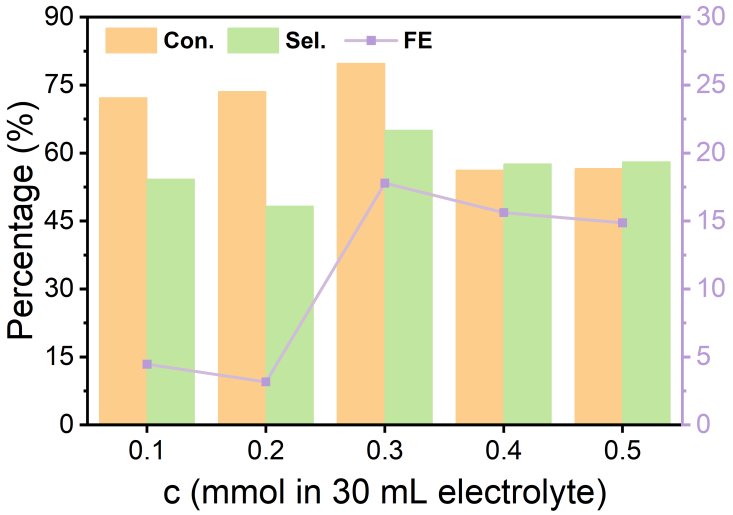

Figure S11. The conversion, selectivity, and Faradaic efficiencies with different concentration of styrene under 1.78 V (*vs.* RHE) using $MnO_2/(Ru_{0.3}Ti_{0.7})O_2$/Ti electrode.

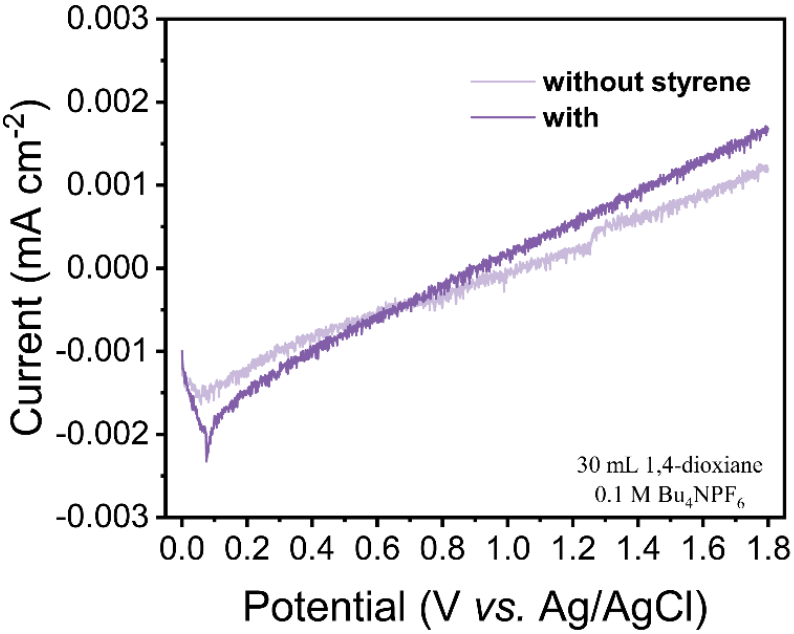

Figure S12. The LSV curves of $MnO_2/(Ru_{0.3}Ti_{0.7})O_2$/Ti in 30 mL 1,4-dioxiane with 0.1 M Bu_4NPF_6 and 0.3 mmol Styrene.

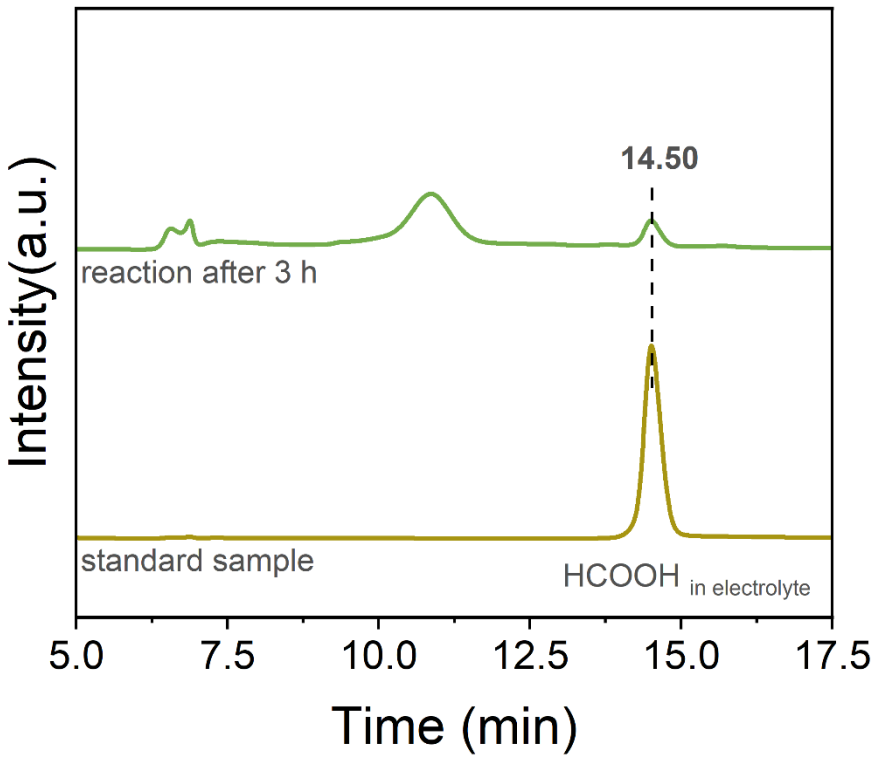

Figure S13. The HPLC chromatograms of reaction mixture and standard sample of formic acid.

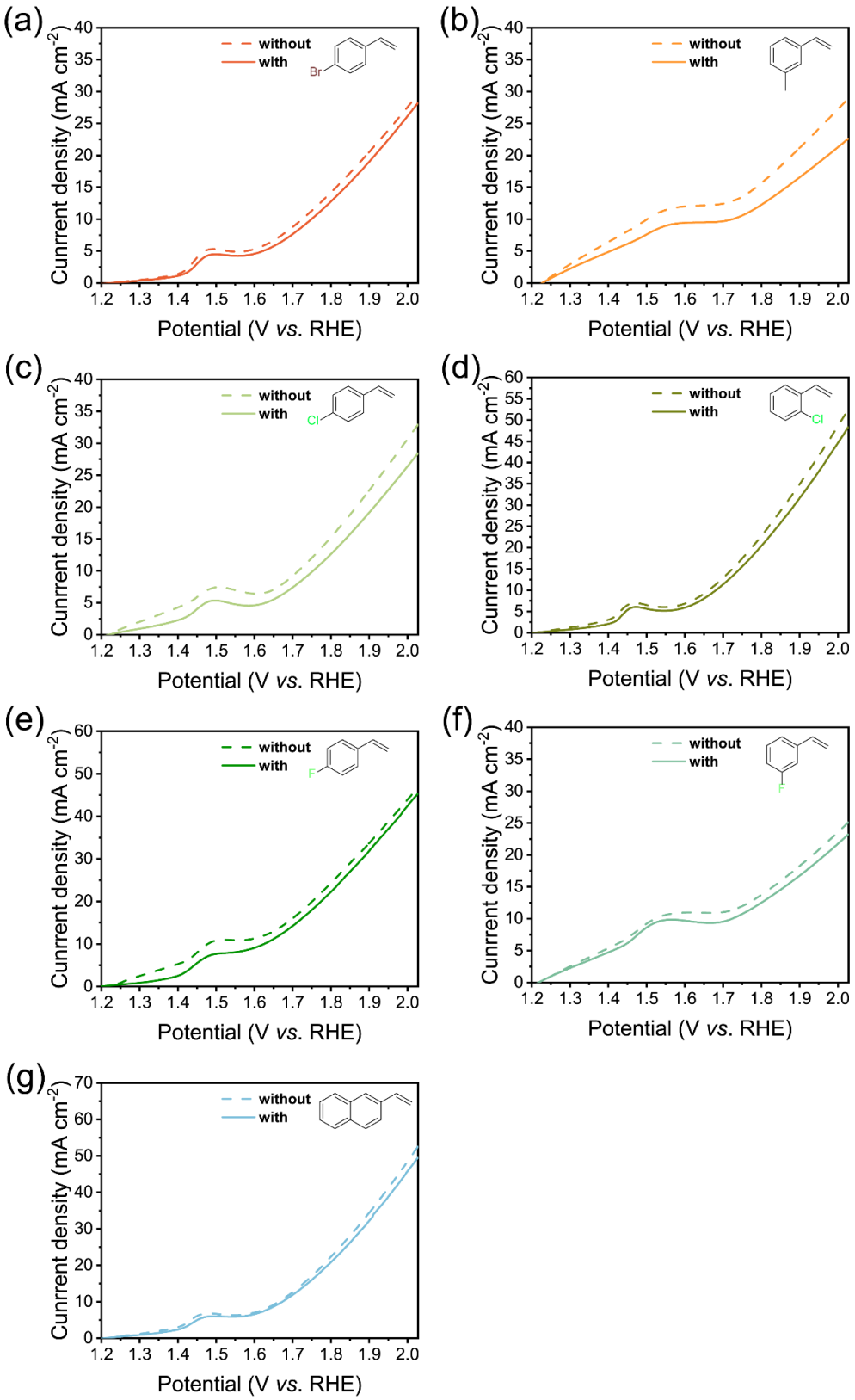

Figure S14. The LSV curves of various substituted aryl olefins at a scan rate of 5 mV s^{-1} using $MnO_2/(Ru_{0.3}Ti_{0.7})O_2/Ti$ in 0.5 M H_2SO_4 and 1,4-dioxane co-solvents (v_1: v_2 =25:5). (Solid and dashed lines represent the presence and absence of 0.3 mmol of reactant.)

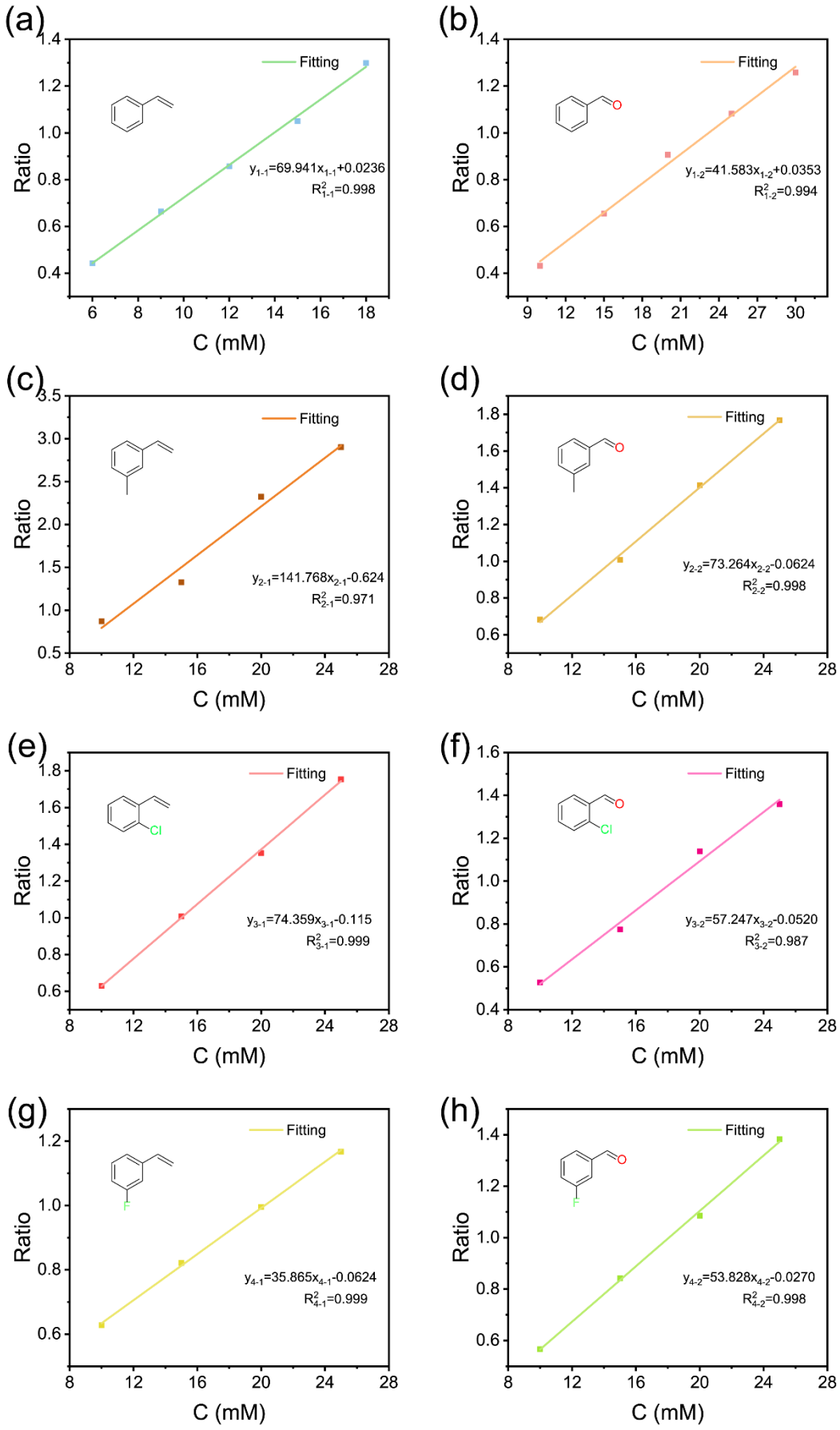

Figure S15. (a-h) Standard curves for various reaction substrates and products.

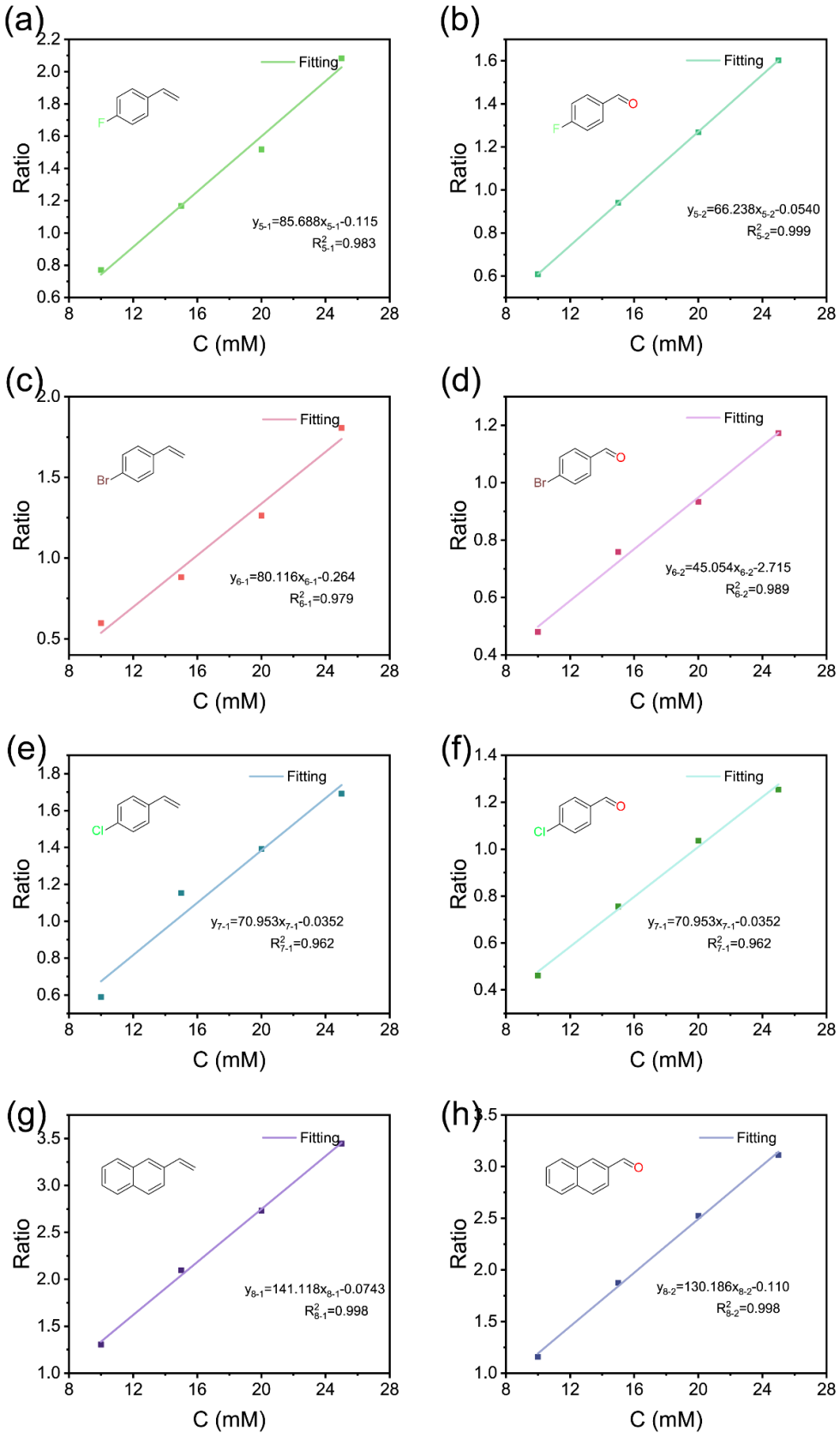

Figure S16. (a-h) Standard curves for various reaction substrates and products.

3. NMR data

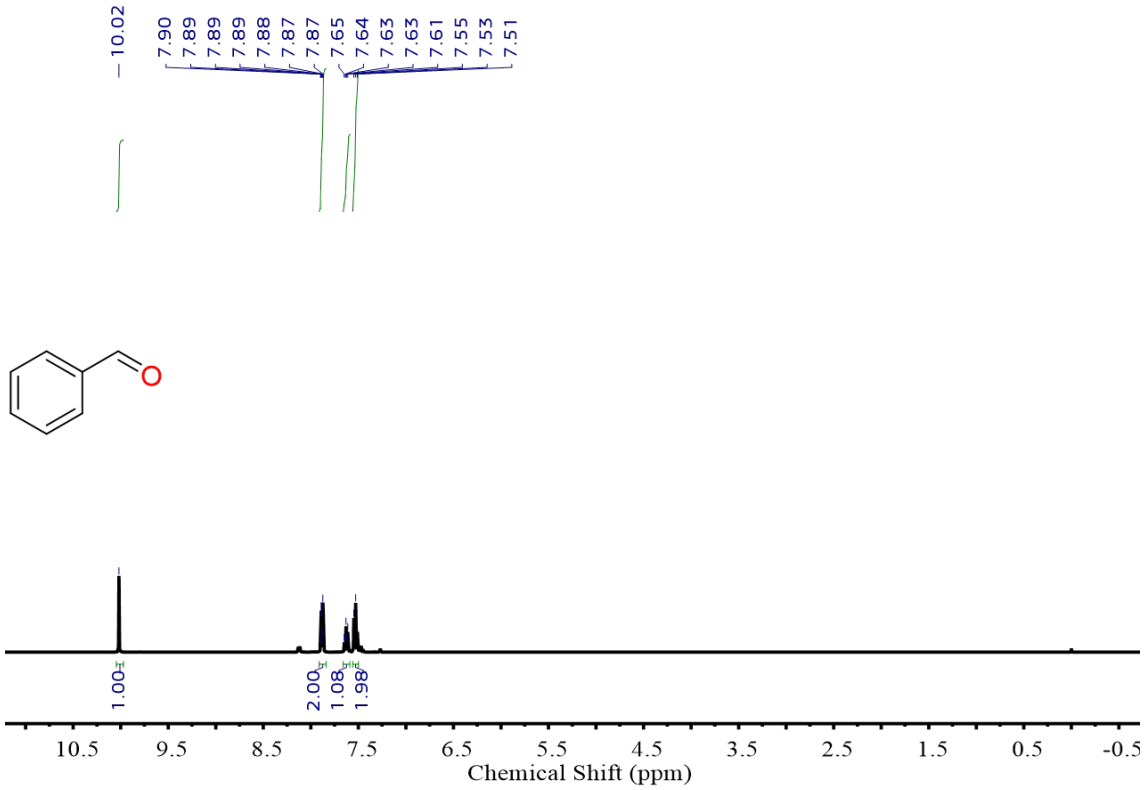

^{1}H NMR (400 MHz, $CDCl_3$) δ 10.02 (s, 1H), 7.90-7.87 (m, 2H), 7.65-7.61(m, 1H), 7.5-7.51 (t, 2H).

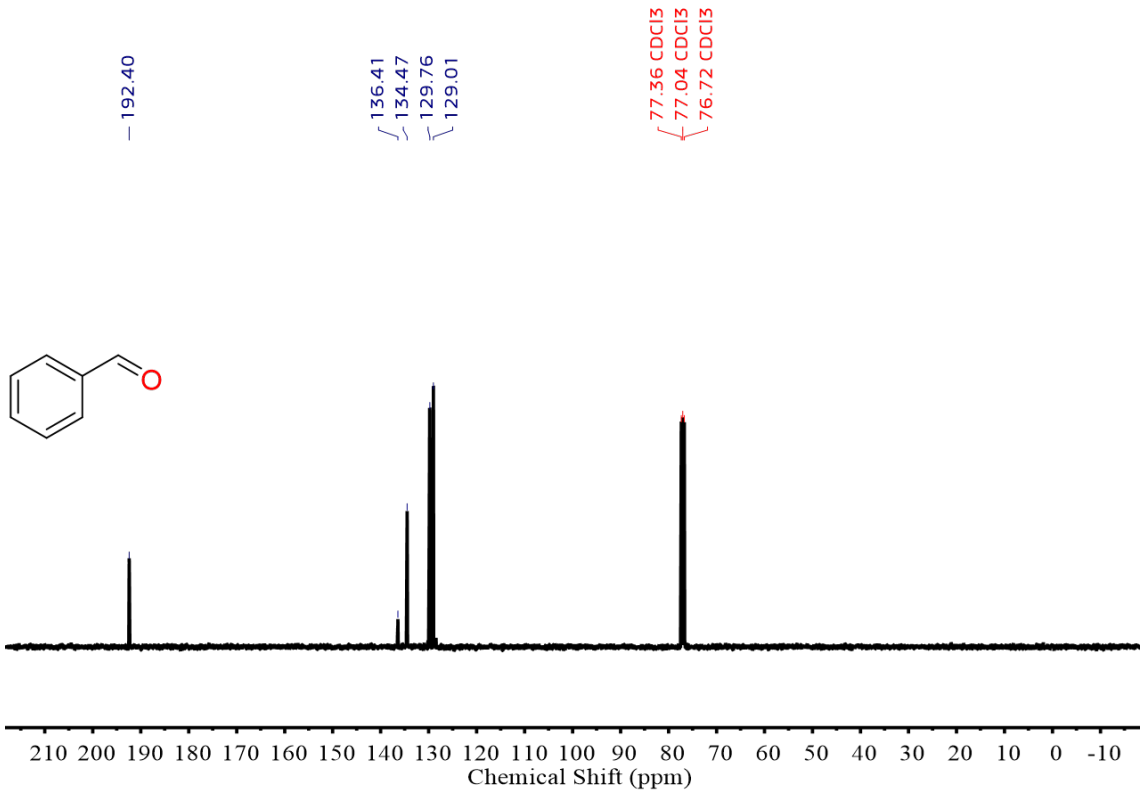

^{13}C NMR (100 MHz, $CDCl_3$) δ 192.40, 136.41, 134.7, 129.76, 129.01, 77.36, 77.04, 76.72.

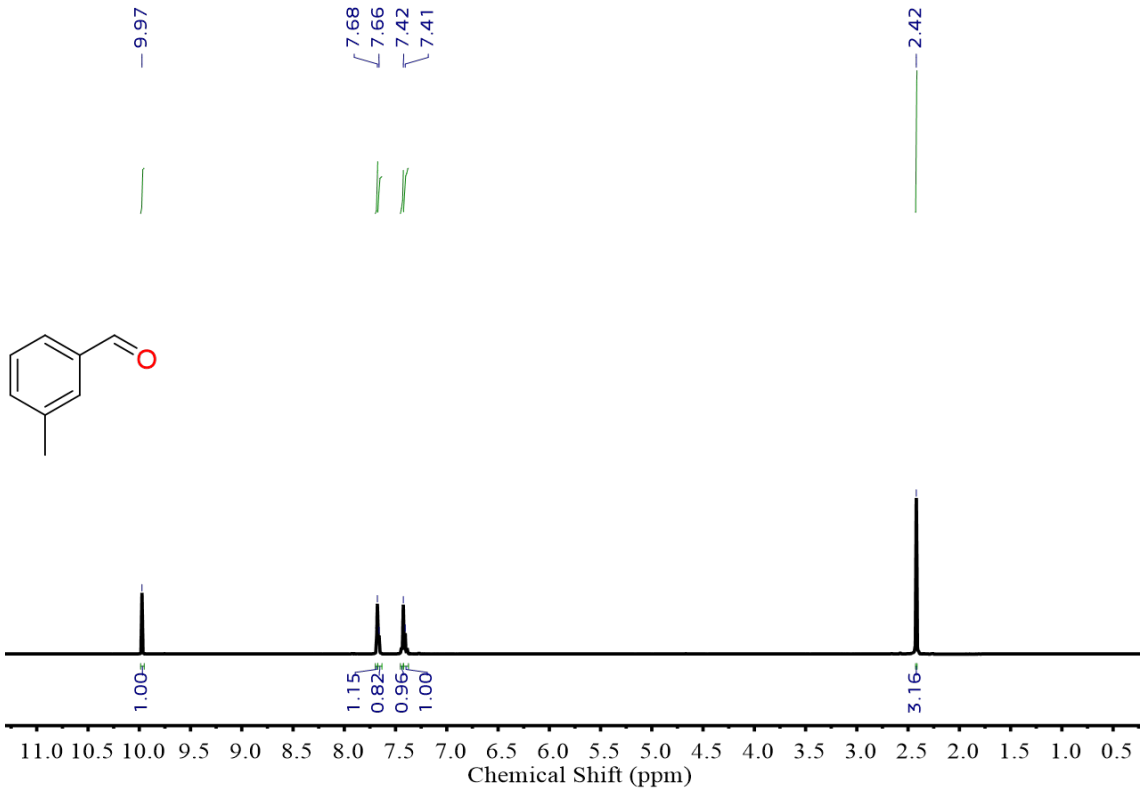

^{1}H NMR (400 MHz, $CDCl_3$) δ 9.97 (s, 1H), 7.68 (s, 1H), 7.66(s, 1H), 7.42 (s, 1H), 7.41 (s, 1H), 2.42(s, 3H).

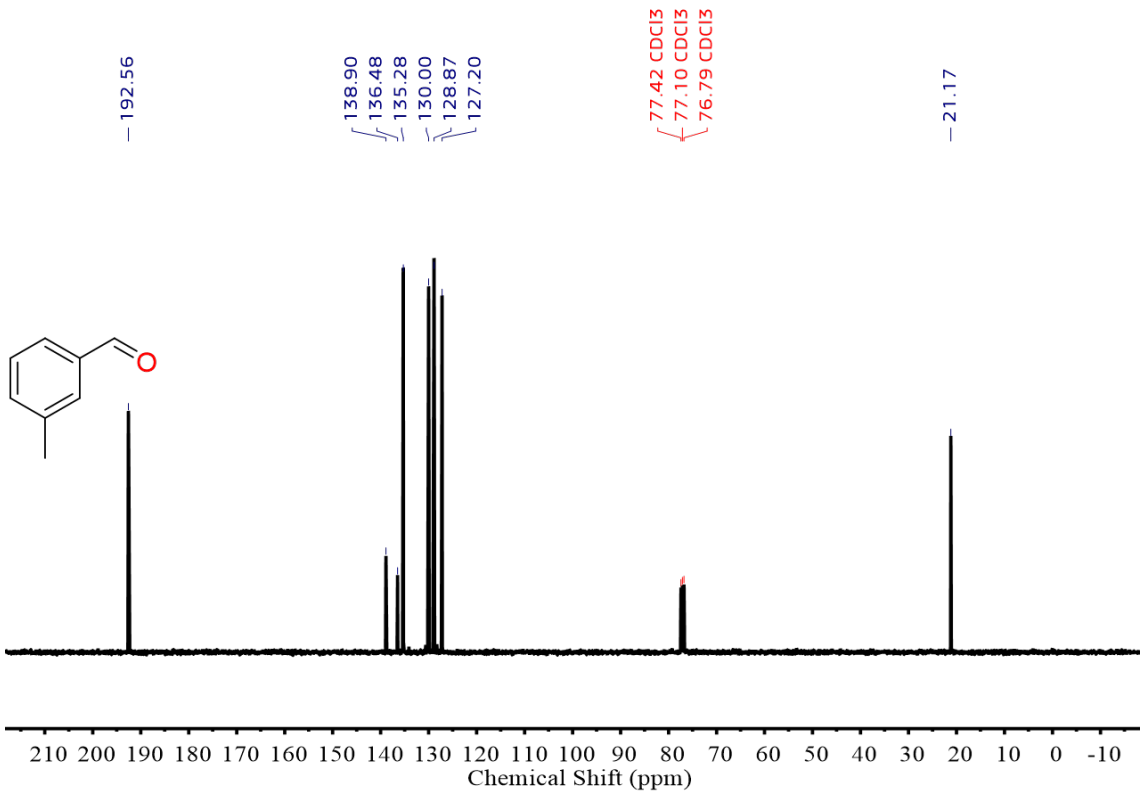

^{13}C NMR (100 MHz, $CDCl_3$) δ 192.56, 138.90, 136.48, 135.28, 130.00, 128.87, 127.20, 77.42, 77.10, 76.79, 21.17.

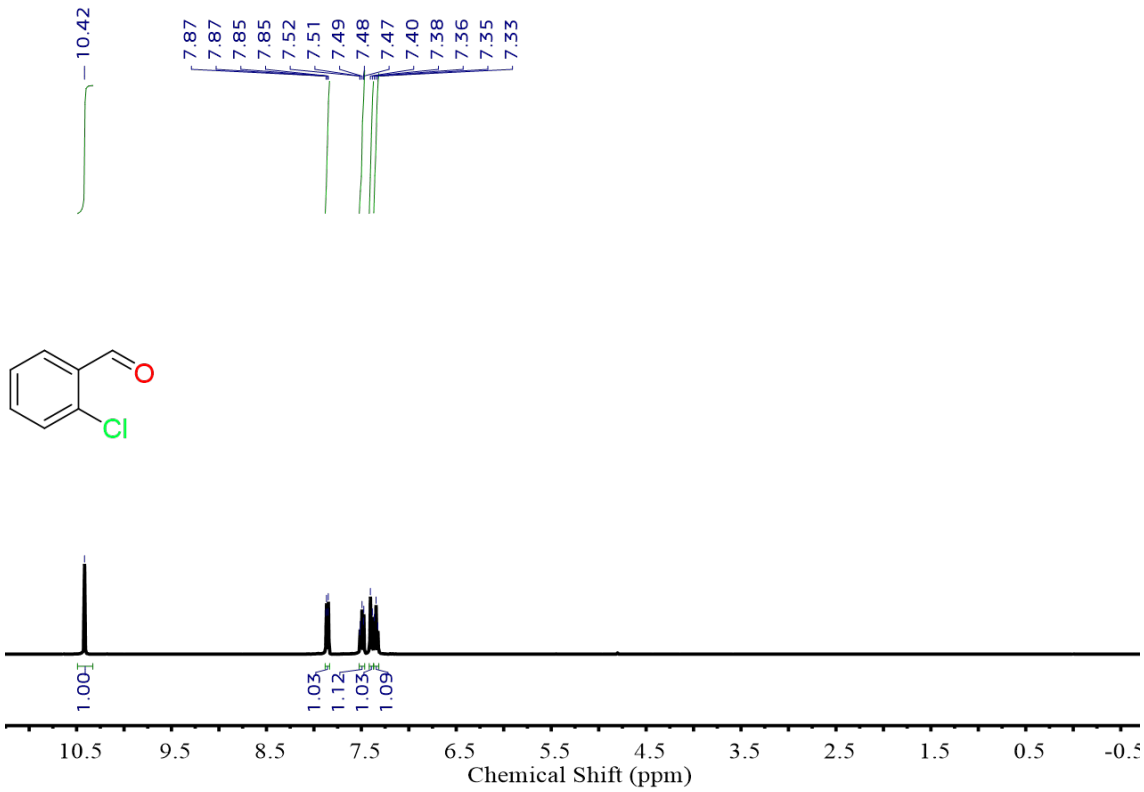

^{1}H NMR (400 MHz, $CDCl_3$) δ 10.42 (s, 1H), 7.87-7.85 (m, 1H), 7.52-7.47 (m, 1H), 7.40-7.36 (t, 1H), 7.35-7.33 (d, 1H).

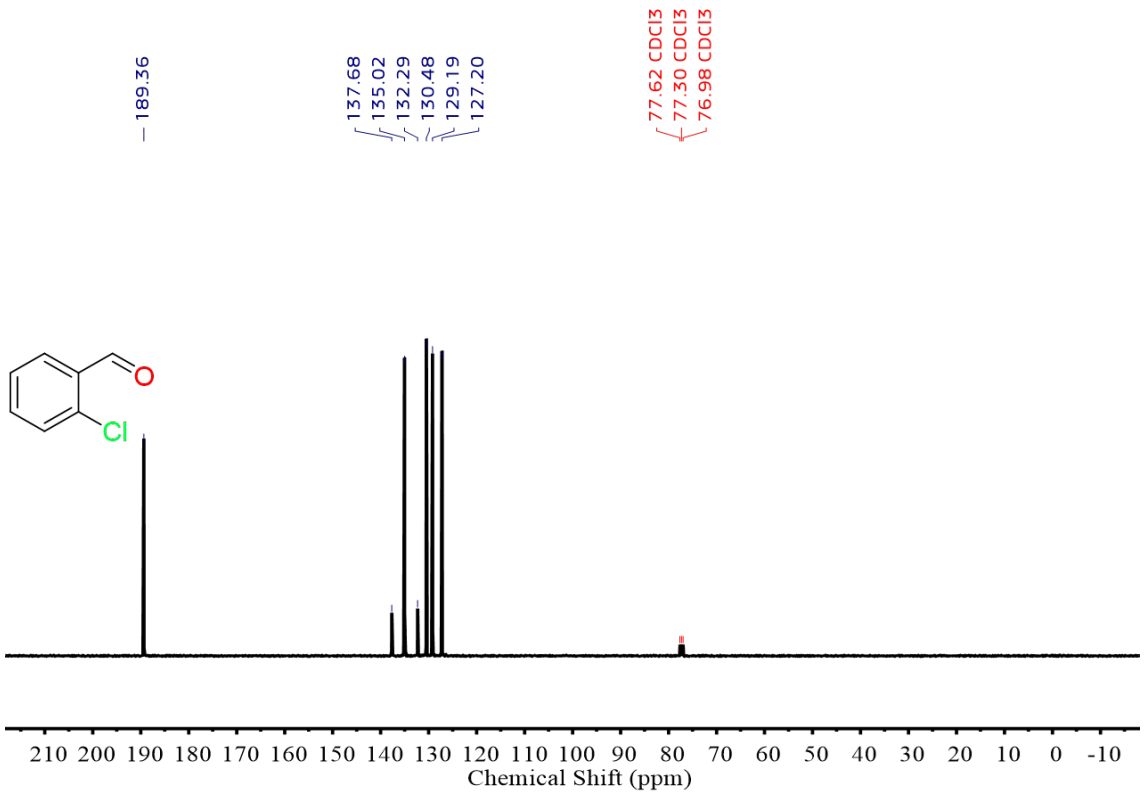

^{13}C NMR (100 MHz, $CDCl_3$) δ 189.36, 137.68, 135.02, 132.29, 130.48, 129.19, 127.20, 77.62, 77.30, 76.89.

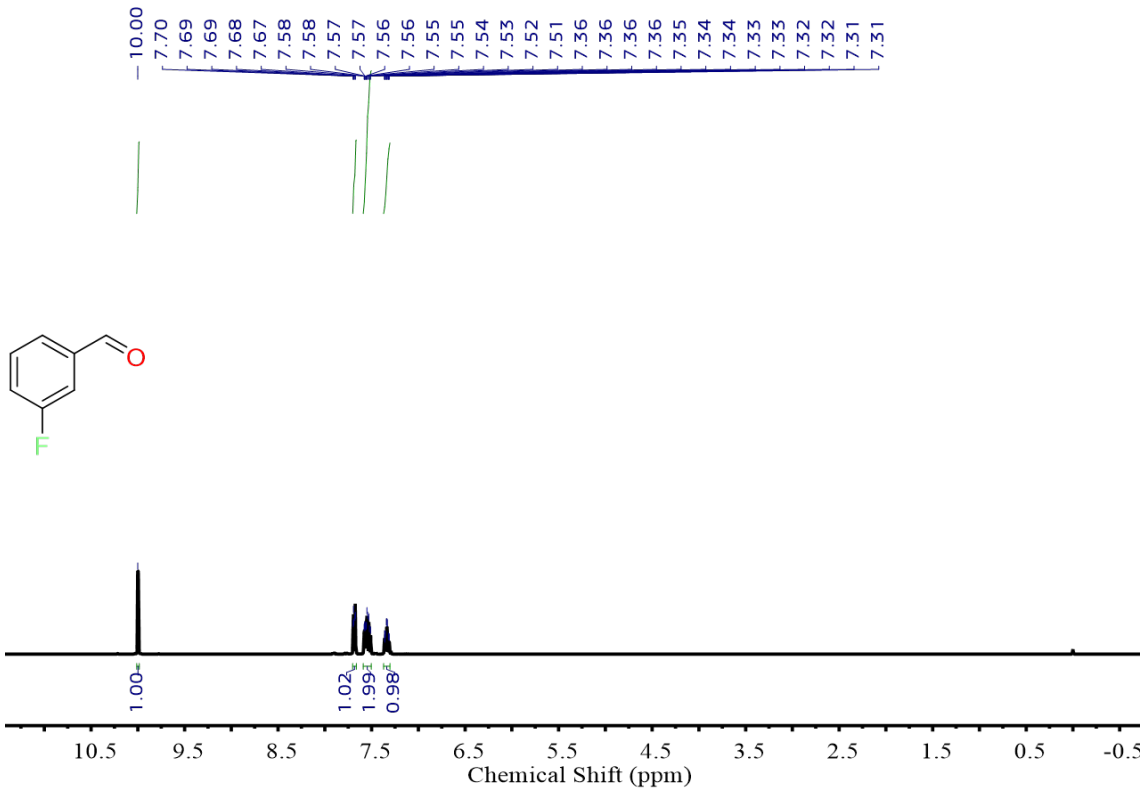

^{1}H NMR (400 MHz, $CDCl_3$) δ 10.00 (s,1H), 7.70-7.67 (m, 1H), 7.58-7.51 (m. 2H), 7.36-7.31 (m, 1H).

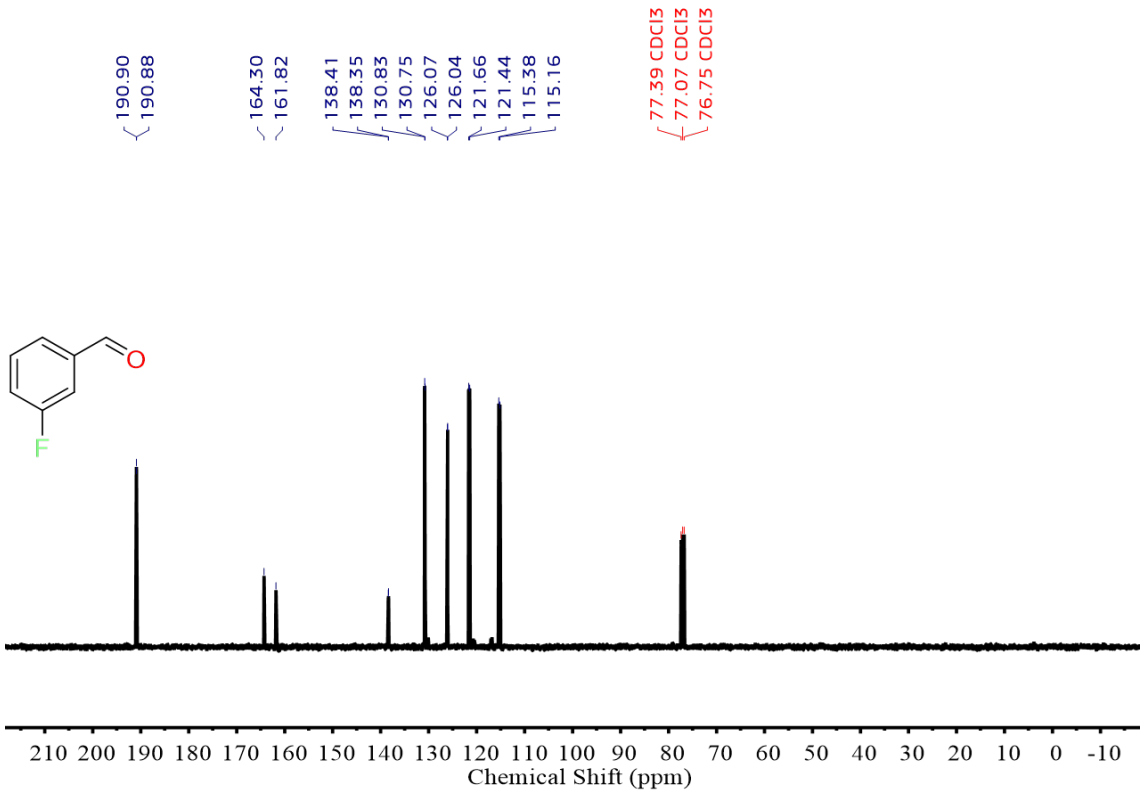

^{13}C NMR (100 MHz, $CDCl_3$) δ 190.90, 190.88, 164.30, 161.82, 138.41, 138.35, 130.83, 130.75, 126.07, 126.04, 121.66, 121.44, 115.38, 115.16.

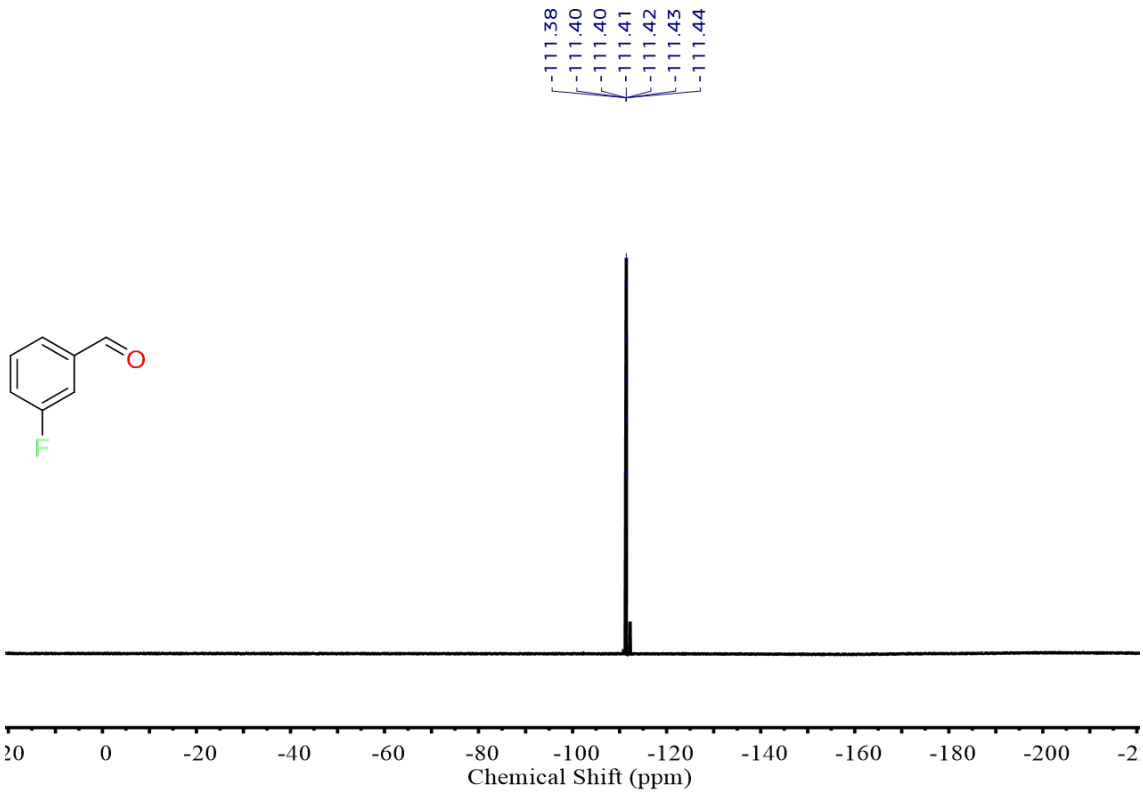

^{19}F NMR (376 MHz, $CDCl_3$) δ -111.38- -111.44.

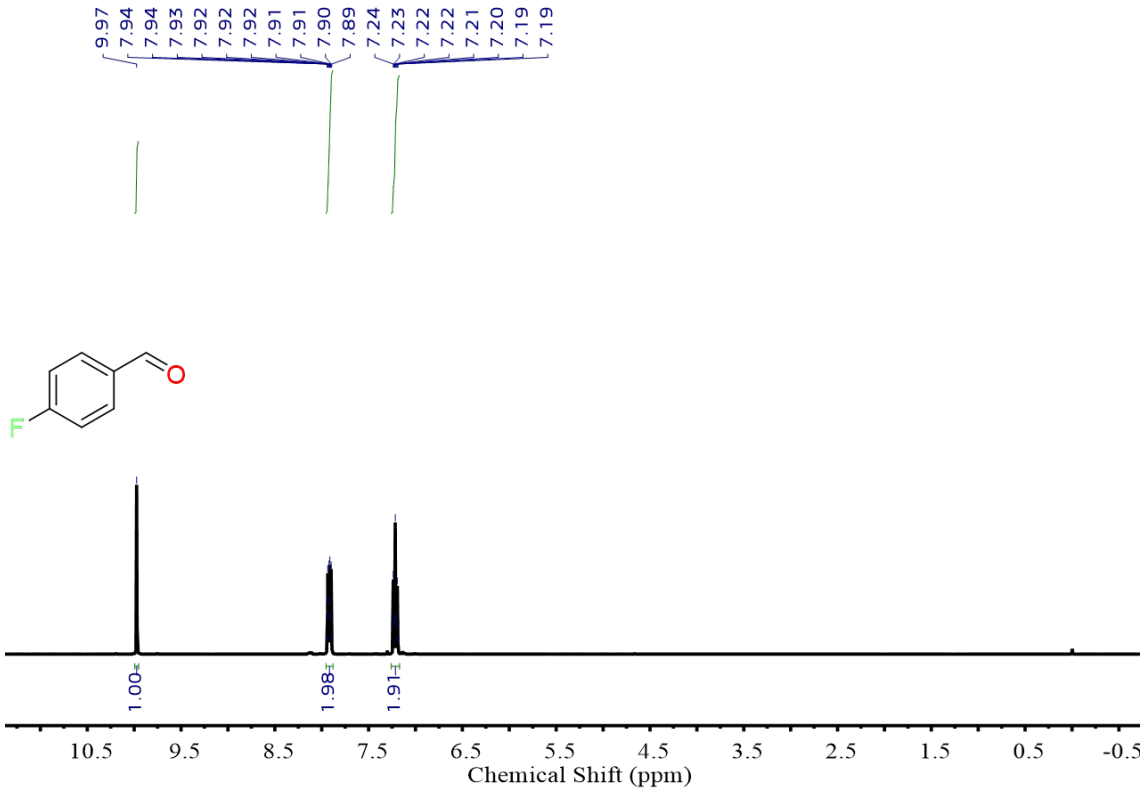

^{1}H NMR (400 MHz, $CDCl_3$) δ 9.97 (s,1H), 7.94-7.89 (m, 2H), 7.24-7.19 (m, 2H).

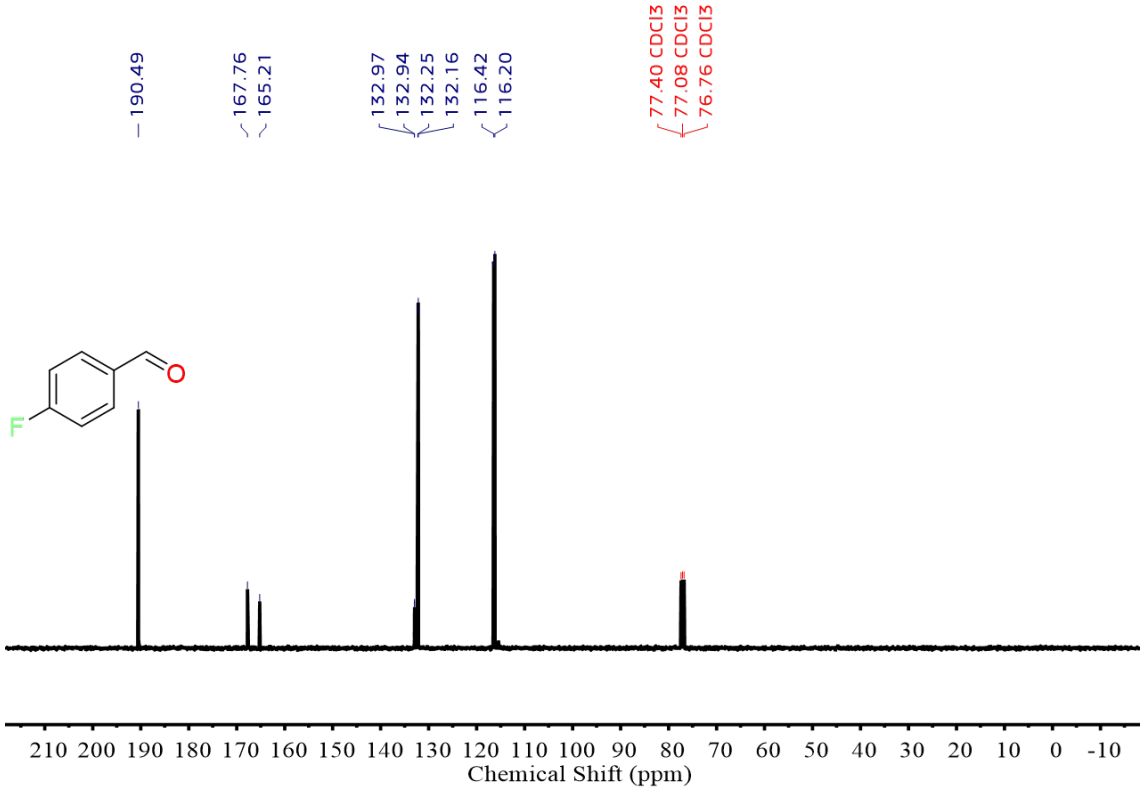

^{13}C NMR (100 MHz, $CDCl_3$) δ 190.49, 167.76, 165.21, 132.97, 132.94, 132.25, 132.16, 116.42, 116.20, 77.40, 77.08, 76.76.

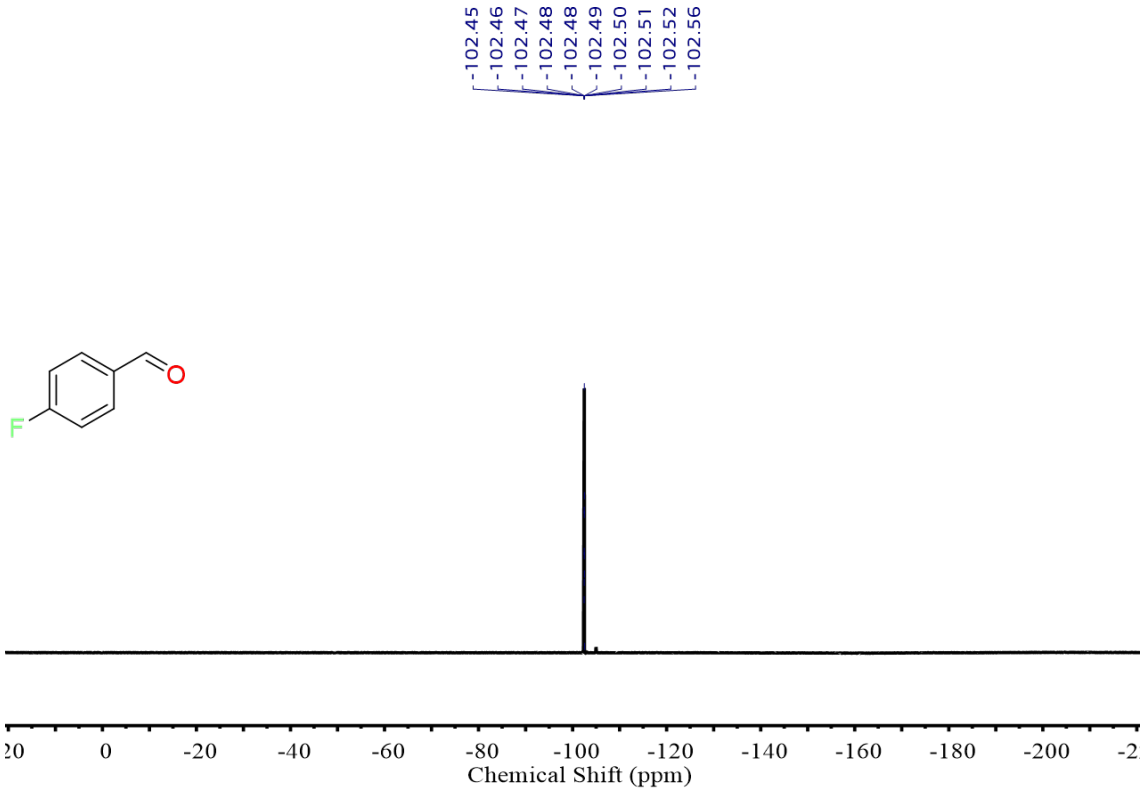

^{19}F NMR (376 MHz, $CDCl_3$) δ -102.45- -102.56.

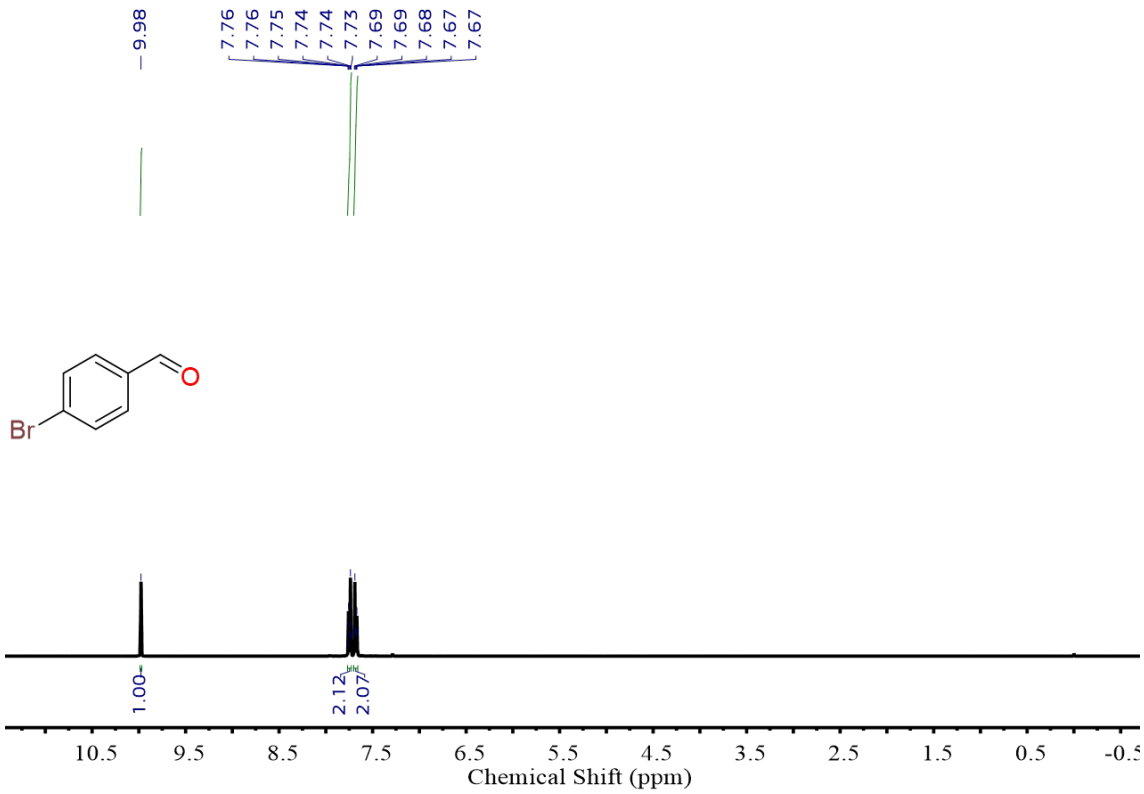

^{1}H NMR (400 MHz, $CDCl_3$) δ 9.98 (s,1H), 7.76-7.73 (m, 2H), 7.69-7.67 (m, 2H).

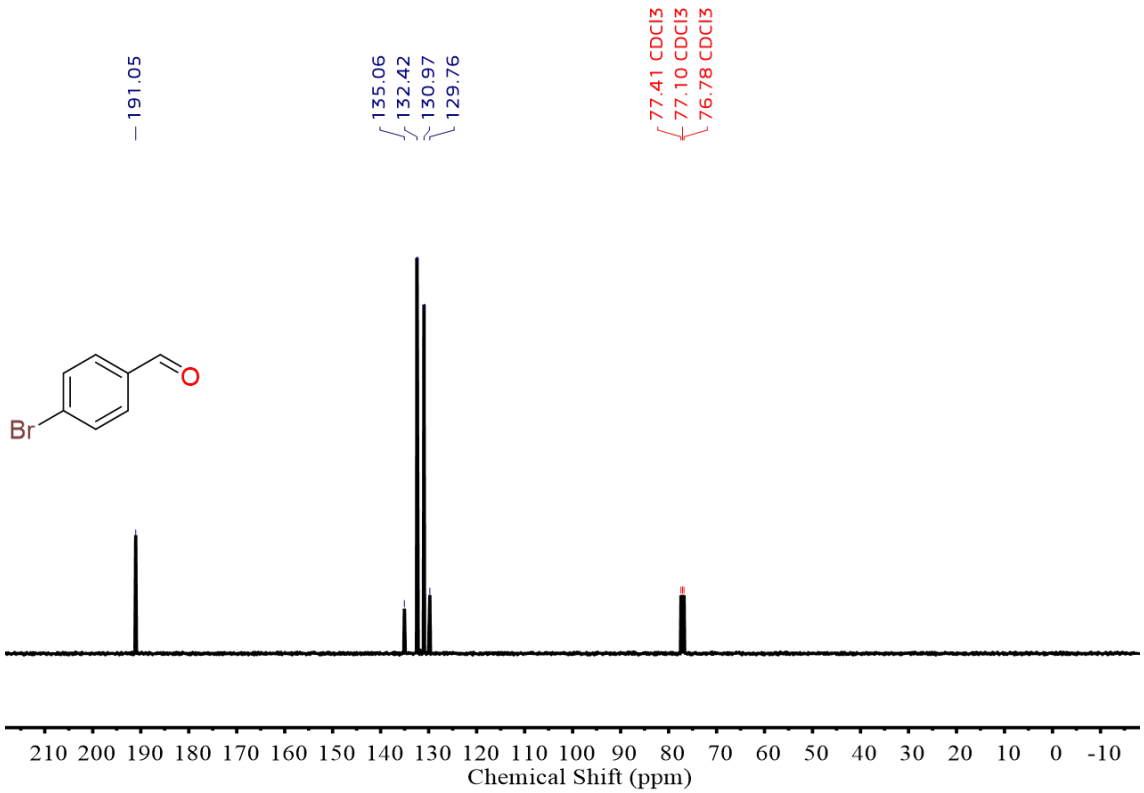

^{13}C NMR (100 MHz, $CDCl_3$) δ 191.05, 135.06, 132.42, 130.97, 129.76, 77.41, 77.10, 76.78.

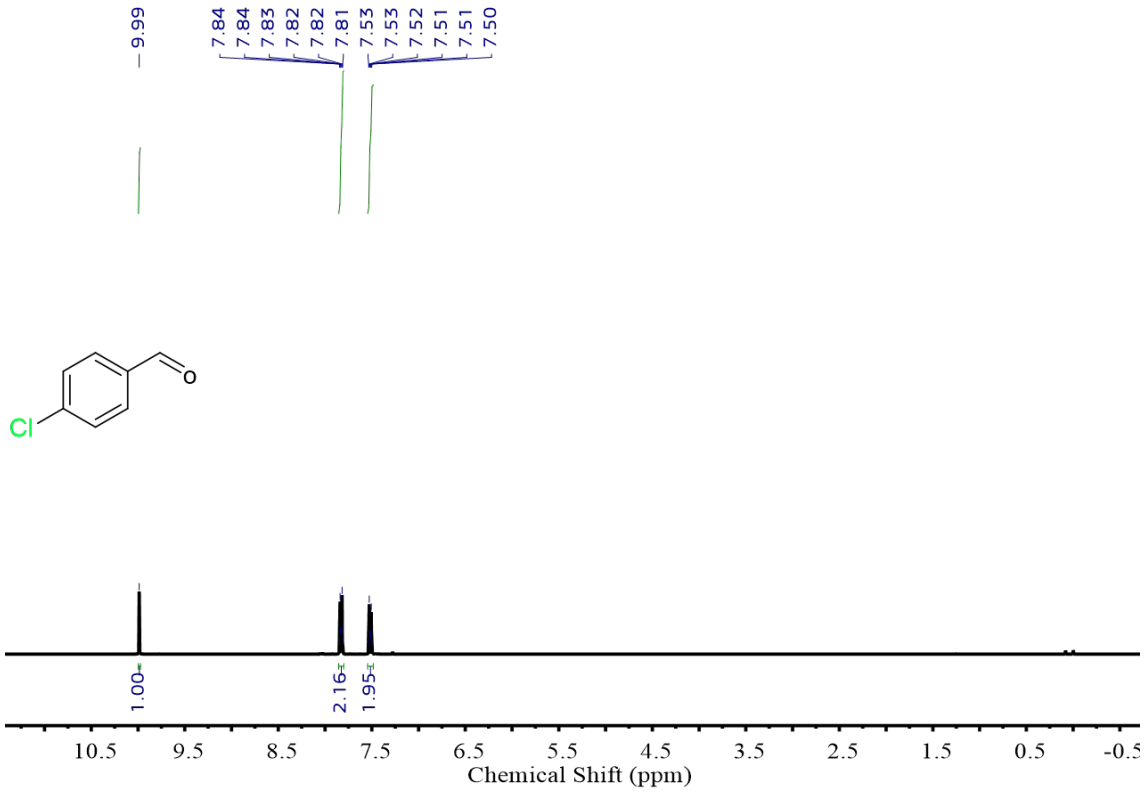

^{1}H NMR (400 MHz, $CDCl_3$) δ 9.99 (s,1H), 7.84-7.81 (m, 2H), 7.53-7.50 (m, 2H).

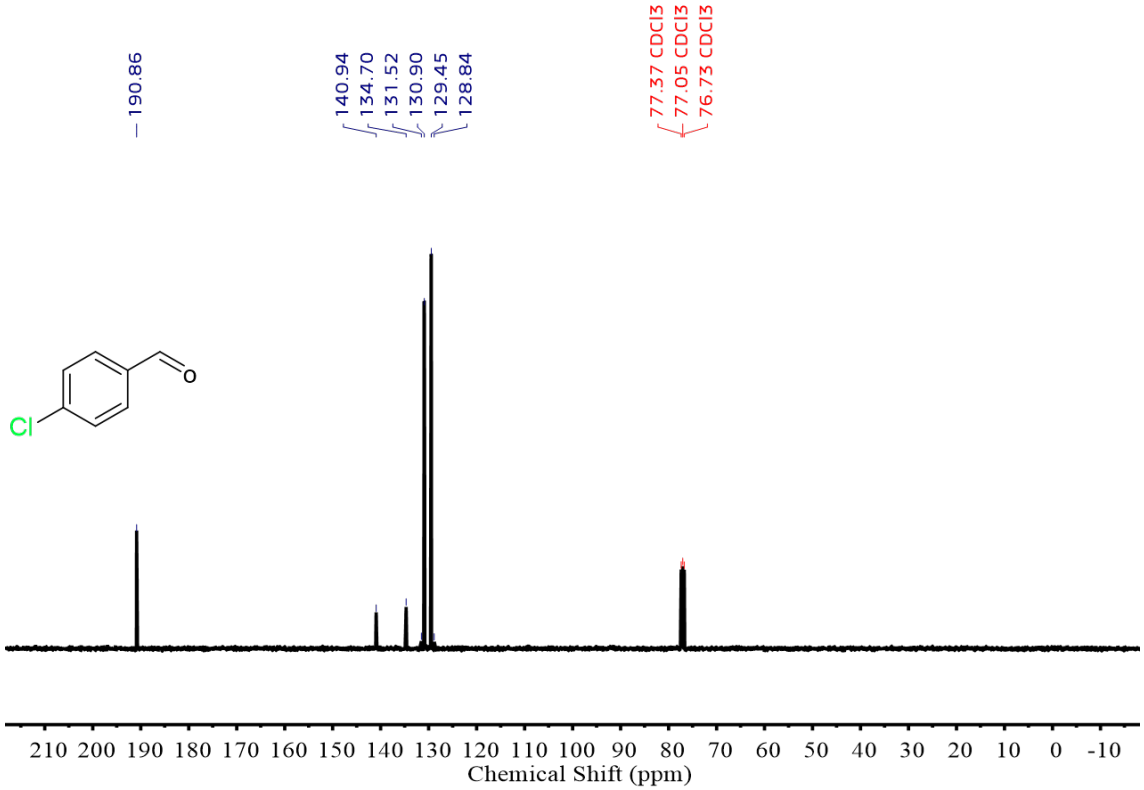

^{13}C NMR (100 MHz, $CDCl_3$) δ 190.86, 140.94, 134.70, 131.52, 130.90, 129.45, 128.84, 77.37, 77.05, 76.73.

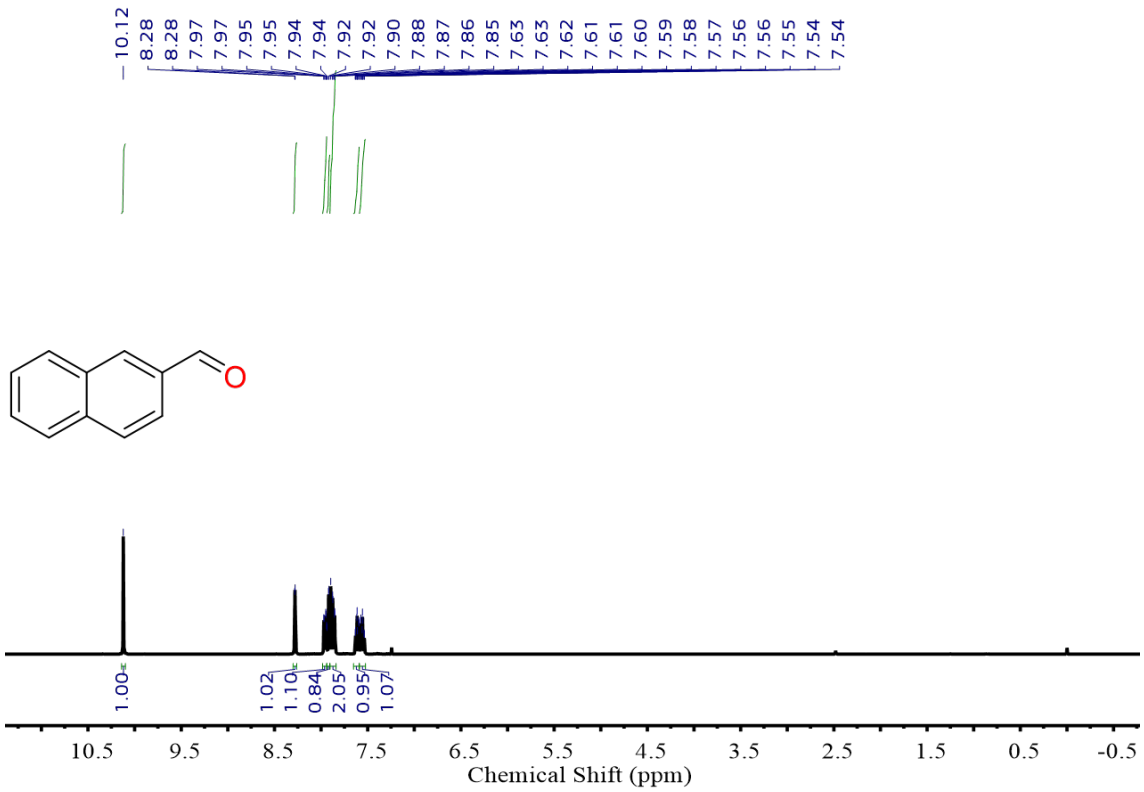

^{1}H NMR (400 MHz, $CDCl_3$) δ 10.12 (s,1H), 8.28 (s, 1H), 7.97-7.94 (m, 1H), 7.92-7.90 (m, 1H), 7.88-7.85 (m, 2H), 7.63-7.59 (m, 1H), 7.58-7.54 (m, 1H).

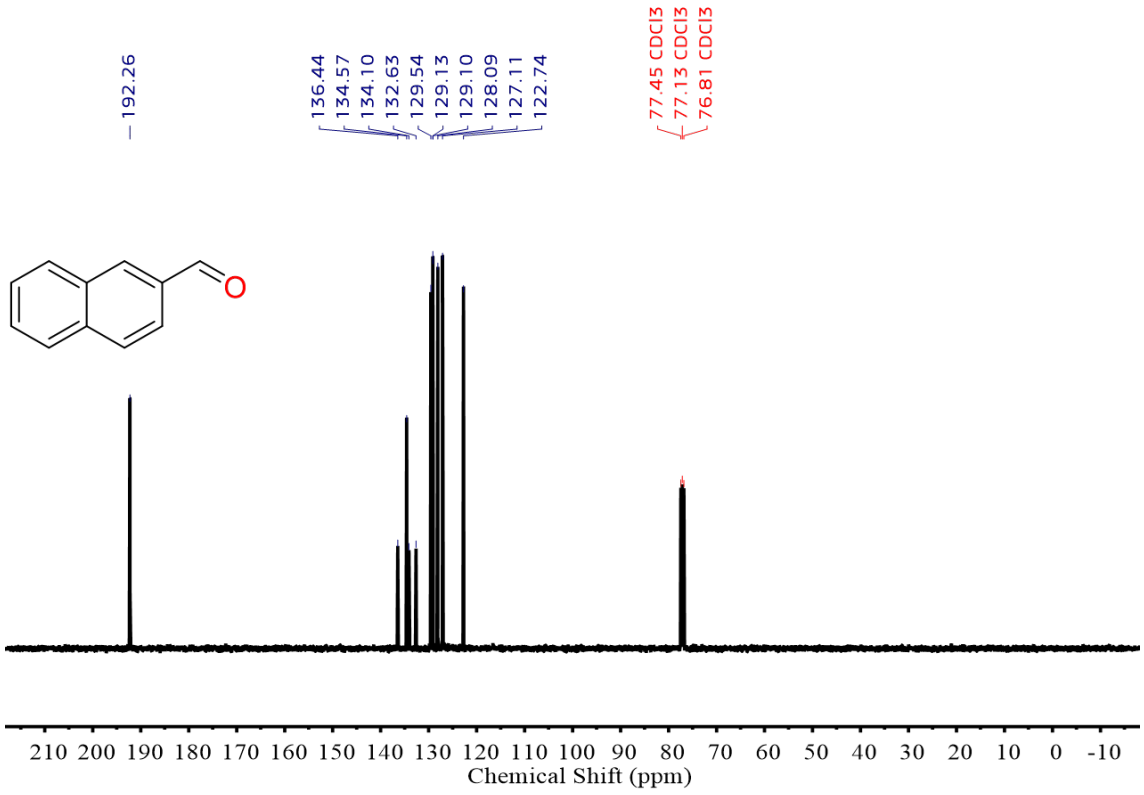

^{13}C NMR (100 MHz, $CDCl_3$) δ 192.26, 136.44, 134.57, 134.10, 132.63, 129.54, 129.13, 129.10, 128.09, 127.11, 122.74, 77.45, 77.13, 76.81.

4. Reference

1. J.-Y. Wang, H.-X. Zhang, K. Jiang and W.-B. Cai, From HCOOH to CO at Pd Electrodes: A Surface-Enhanced Infrared Spectroscopy Study, *Journal of the American Chemical Society*, 2011, **133**, 14876-14879.
2. H. A. P., Efficient ab initio tight binding, *The American Physical Society*, 1997, **56**, 6594-6602.
3. J. P. Perdew, K. Burke and M. Ernzerhof, Generalized gradient approximation made simple, *Physical Review Letters*, 1996, **77**, 3865-3868.
4. G. Kresse and J. Furthmüller, Efficiency of ab-initio total energy calculations for metals and semiconductors using a plane-wave basis set, *Computational Materials Science*, 1996, **6**, 15-50.
5. S. Grimme, J. Antony, S. Ehrlich and H. Krieg, A consistent and accurate ab initio parametrization of density functional dispersion correction (DFT-D) for the 94 elements H-Pu, *The Journal of Chemical Physics*, 2010, **132**, 154104.